Journal of Catalysis **184,** 357–376 (1999)
Article ID jcat.1999.2420, available online at http://www.idealibrary.com on IDEAL®

A Mechanistic Study of Methanol Decomposition over Cu/SiO_2, ZrO_2/SiO_2, and $Cu/ZrO_2/SiO_2$

Ian A. Fisher and Alexis T. Bell

Chemical Sciences Division, Lawrence Berkeley National Laboratory, and Department of Chemical Engineering, University of California, Berkeley, California 94720-1462

Received October 2, 1998; revised December 29, 1998; accepted January 13, 1999

The interaction of methanol with Cu/SiO_2, ZrO_2/SiO_2, and $Cu/ZrO_2/SiO_2$ has been investigated by *in situ* infrared spectroscopy and temperature programmed desorption and reaction with the aim of understanding the nature of the species and the mechanism involved in methanol decomposition. In the case of Cu/SiO_2, methanol exposure results in the formation of methoxide species on Cu and SiO_2 at 323 K. In the absence of methanol in the gas phase, methoxide species on Cu are dehydrogenated to give formaldehyde starting at ~340 K and are oxidized to formate species at ~373 K, which then decomposes to CO_2 and H_2 at ~390 K. When methanol is present in the gas phase, methyl formate, CO, and H_2, resulting from the decomposition of methyl formate, are formed in addition to the above reactions. When ZrO_2/SiO_2 or $Cu/ZrO_2/SiO_2$ is exposed to methanol, the majority of the surface species observed are associated with zirconia. Methanol adsorption on either ZrO_2/SiO_2 or $Cu/ZrO_2/SiO_2$ leads to methoxide formation on zirconia and SiO_2 at 323 K. In the presence of Cu, methoxide species on zirconia are dehydrogenated to give formaldehyde starting at ~325 K, which is oxidized to formate species on zirconia at ~373 K, which decompose to CO, CO_2, and H_2 at ~400 K. Methyl formate and dimethyl ether are also observed to form above 460 K. In the absence of Cu, methoxide species on zirconia decompose only very slowly at 523 K. Metallic Cu is proposed to provide sites on which hydrogen atoms formed during the dehydrogenation of species located on zirconia can recombine efficiently and desorb as H_2. Thus, methanol decomposition over $Cu/ZrO_2/SiO_2$ is envisioned to occur primarily on ZrO_2, with the primary function of Cu being the removal of hydrogen.

INTRODUCTION

Catalysts containing Cu and zirconia have been observed to be significantly more active for methanol synthesis from CO/H_2 and CO_2/H_2 than catalysts containing Cu or zirconia alone (1–12). In previous mechanistic studies of methanol synthesis from CO/H_2 and CO_2/H_2, we have observed that catalysts containing Cu and zirconia behave in a bifunctional manner, with Cu and zirconia having complementary but different roles (13, 14). Zirconia provides adsorption sites for CO and CO_2, and is the location of all carbon containing intermediates leading to methanol. Copper serves to dissociate molecular hydrogen and supply atomic hydrogen by spillover to the reactive intermediates located on zirconia. The purpose of the present study is to examine the mechanism by which methanol is decomposed on Cu and zirconia containing catalysts and to determine whether a similar type of bifunctionality is observed during methanol decomposition as is observed during methanol synthesis. To achieve this objective, the interactions of methanol with Cu/SiO_2, ZrO_2/SiO_2, and $Cu/ZrO_2/SiO_2$ were investigated using *in situ* FTIR spectroscopy under both steady-state and transient conditions. Temperature programmed desorption (TPD) and temperature programmed reaction (TPR) of methanol were also performed to identify gas-phase decomposition products and the temperatures at which they are formed.

Previous investigations of methanol adsorption and decomposition have been performed on Cu/SiO_2 (15, 16), ZrO_2 (17–21), and CuO/ZrO_2 (21). Millar *et al.* (15) have reported that methanol adsorption on Cu/SiO_2 at 295 K resulted in the formation of methoxide groups on both Cu and SiO_2. Heating the adsorbed species to 393 K led to the loss of methoxide groups on Cu and the appearance of formate species on Cu. Further heating to 538 K produced gas-phase and adsorbed methyl formate, as well as CO_2 and CO. Clarke *et al.* (16) have also investigated methanol decomposition on Cu/SiO_2. They observed the formation of adsorbed methoxide, formaldehyde, methylenebisoxy, and formate groups on Cu upon methanol adsorption at 303 K, and during temperature-programmed desorption in He, they observed the decomposition of the formate species to CO_2 and H_2 starting at ~430 K.

For zirconia, He and Ekerdt (18) have reported the appearance of methoxide species upon exposure to methanol at 298 K. During temperature-programmed desorption of adsorbed methanol, CO, CH_4, CH_3OH, and CH_2O peaks were observed at ~453 K (17). CO, CO_2, CH_4, H_2, and H_2O were observed at ~773 K, and additional CO and CO_2 formation was observed at ~863 K. Hussein *et al.* (19) have also reported methoxide formation upon exposure of zirconia

0021-9517/99 $30.00

to methanol at room temperature. Methoxide decomposition was found to occur at ~523–573 K, with the formation of CO and CO_2 at higher temperatures.

On CuO/ZrO_2 Bianchi *et al.* (21) have observed bifunctional catalysis during methanol adsorption and decomposition, where zirconia provides adsorption sites for reaction intermediates and Cu is proposed to facilitate the transfer and utilization of hydrogen. Methanol adsorption on CuO/ZrO_2 and ZrO_2 was shown to result in the formation of methoxide species on zirconia at 298 K, which are converted to formate and carbonate species on zirconia and finally to gas-phase CO, CO_2, H_2, and H_2O at higher temperatures. It was observed that the transformation of methoxide species to formate and carbonate species occurs at lower temperatures when Cu is present. The spillover of hydrogen from Cu was envisioned to restore OH groups on zirconia, which react with methoxide, resulting in formate and carbonate formation. In the absence of Cu, OH groups on zirconia are depleted, resulting in less efficient methoxide conversion.

EXPERIMENTAL

The preparation and characterization of the Cu/SiO_2, ZrO_2/SiO_2, and $Cu/ZrO_2/SiO_2$ catalysts used in this study are described in Refs. 12 and 13. The Cu and Zr contents of the catalysts were determined by X-ray fluorescence analysis, and the surface area of the dispersed Cu was determined by N_2O titration (12). The Cu/SiO_2 contains 5.7 wt% Cu and has a Cu surface area of 1.36 m^2/g of catalyst (3.7% Cu dispersion), the ZrO_2/SiO_2 catalyst contains 32.6 wt% ZrO_2, and the $Cu/ZrO_2/SiO_2$ catalyst contains 5.7 wt% Cu, having a Cu surface area of 0.76 m^2/g of catalyst (2.1% Cu dispersion) and 30.5 wt% ZrO_2.

Matheson UHP He was passed through an oxysorb (CrO_2) trap to remove O_2 and then a molecular sieve trap prior to use. Methanol adsorption onto the catalyst was from a UHP argon stream containing 1.0% methanol. The flow rate of each gas was controlled by a Tylan Model FC-280 mass flow controller, and gases were delivered to the catalyst sample at atmospheric pressure.

In situ transmission infrared spectroscopy was performed using 2-cm-diameter catalyst disks of 0.2 mm thickness, weighing approximately 75 mg. The catalyst disks were contained in a low dead-volume infrared cell (22). The cell was heated by electrical resistance heaters and the cell temperature was controlled by an Omega Series CN-2010 programmable temperature controller. Infrared spectra were collected using a Nicolet Magna 750 Series II FTIR spectrometer equipped with a narrow band MCT detector. To achieve good signal-to-noise ratios, 64 scans at 4 cm^{-1} resolution were averaged. Each spectrum was then referenced to a spectrum of the reduced catalyst (see below) collected at the same temperature in flowing He. An experiment was initiated by exposing the reduced catalyst to 1% methanol in Ar flowing at 60 cm^3/min for 30 min and then purging in He flowing at 60 cm^3/min for 30 min at 323 K, 373 K, 423 K, 473 K, and 523 K. Spectra were collected after exposure to flowing methanol for 30 min and after He purging for 30 min.

TPD of methanol was performed in a microreactor by exposing the reduced catalyst to 1% methanol in Ar flowing at 60 cm^3/min for 30 min at room temperature. The sample was then purged at room temperature in He flowing at 60 cm^3/min for 1 h, after which the temperature was increased linearly at 4 K/min, while continuing to flow He at 60 cm^3/min. TPR of methanol was performed by exposing the reduced catalyst to 1% methanol in Ar flowing at 60 cm^3/min for 30 min at room temperature, after which the temperature was increased linearly at 4 K/min, while continuing to flow 1% methanol in Ar at 60 cm^3/min. The microreactor was heated by electrical resistance heaters and the reactor temperature was controlled by an Omega Series CN-2010 programmable temperature controller. Gas-phase product compositions were determined using a quadrupole mass spectrometer (UTI 100C). Approximately 150 mg of catalyst was used in the TPD and TPR experiments.

Prior to each experiment with a fresh sample, the catalyst was reduced in 10% H_2/He flowing at 60 cm^3/min. The reduction temperature was raised at 2 K/min from ambient to 523 K, after which the catalyst was further reduced at 523 K for >8 h in pure H_2 flowing at 40 cm^3/min. Subsequent reductions were all performed at 523 K, but varied in time (always >8 h), to ensure that observable surface species were removed. Following the treatment in hydrogen, the catalyst was purged in He flowing at 60 cm^3/min at 523 K for 1 h to remove hydrogen from the sample.

RESULTS

Observations of Surface Species by Infrared Spectroscopy

Cu/SiO_2. Figure 1 shows infrared spectra taken 30 min after Cu/SiO_2 was exposed to a stream of 1% methanol in Ar at temperatures between 323 and 523 K and 1 atm total pressure. Also shown are spectra taken after purging the catalyst in He for 30 min at each temperature. At 323 K in flowing methanol, the C–H stretching region shows maxima at 2998, 2956, 2926, 2897, 2853, and 2814 cm^{-1}. Upon purging, the peaks at 2956 and 2853 cm^{-1} decrease most significantly in intensity and shift to 2961 and 2861 cm^{-1}, respectively. The bands at 2956 and 2853 cm^{-1} are assigned to physisorbed methanol on SiO_2 (15, 16), the bands at 2998, 2961, and 2861 cm^{-1} to methoxide on silica (CH_3O–Si) (13–16, 23, 24), and the bands at 2926, 2897, and 2814 cm^{-1} to methoxide on Cu (CH_3O–Cu) (14–16). At lower wavenumbers, we observe the bending modes of

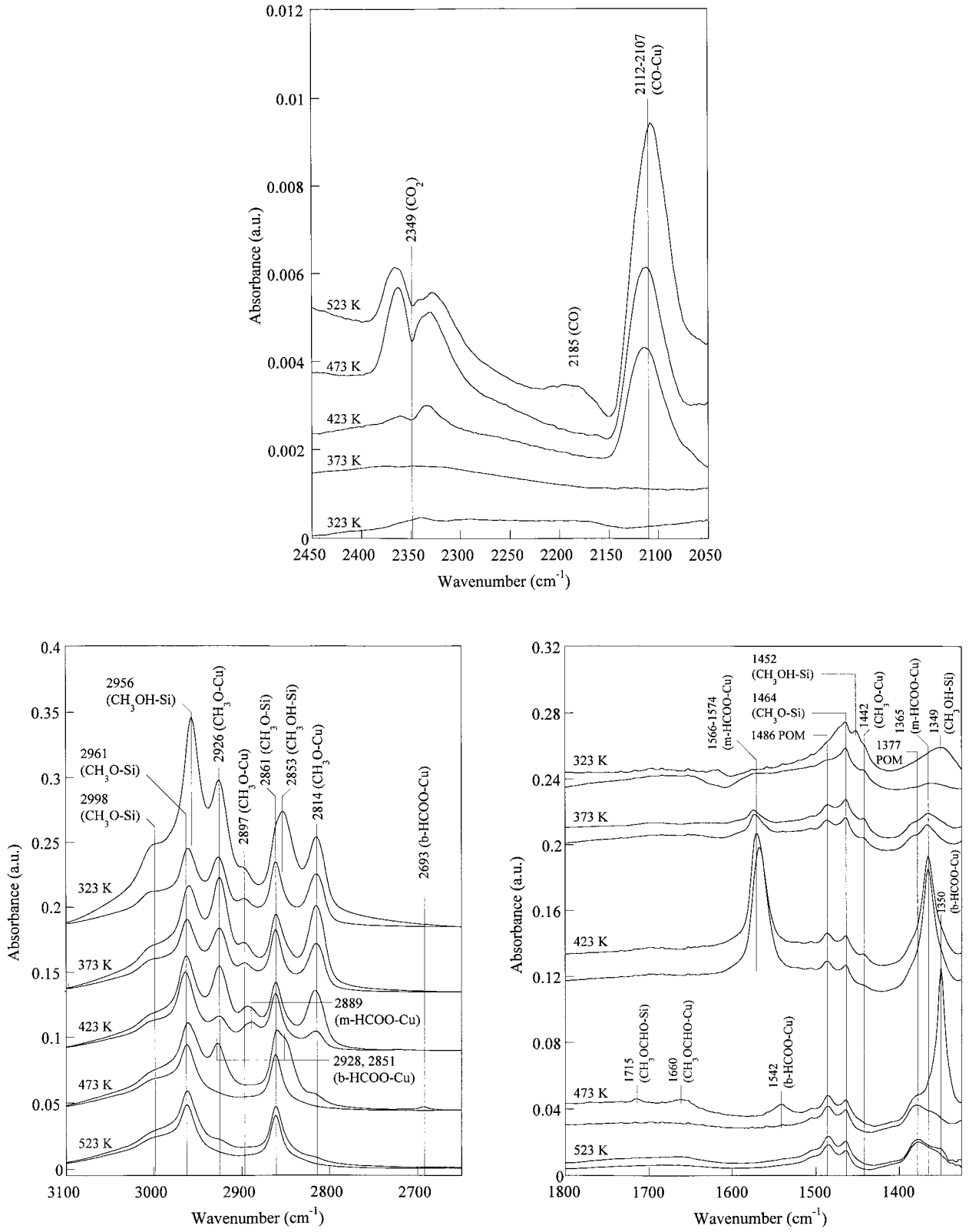

FIG. 1. Infrared spectra taken during exposure of Cu/SiO_2 to a stream of 1% methanol in Ar flowing at 60 cm^3/min for 30 min at atmospheric pressure (top spectrum at each temperature) and after exposure to He flowing at 60 cm^3/min for 30 min at atmospheric pressure (bottom spectrum at each temperature). In the region 2450–2050 cm^{-1}, only spectra taken during methanol exposure are shown. Spectra referenced to reduced Cu/SiO_2 under atmospheric pressure He flow at each temperature.

CH_3O–Si at 1464 cm^{-1} (14, 23, 24), CH_3O–Cu (1442 cm^{-1}) (14, 15), and physisorbed methanol on SiO_2 (1452 cm^{-1}) (16), as well as the broad band at 1349 cm^{-1} attributed to OH in-plane bending of adsorbed methanol (15).

The spectrum observed at 373 K is similar to that seen at 323 K, but new features appear at 1486 and 1377 cm^{-1}. These bands continue to grow with time and temperature and are characteristic of a polymerized form of formaldehyde (polyoxymethylene (POM)) observed during CO hydrogenation on Cu/SiO_2 (14) and during methanol interaction with Cu/SiO_2 (23). Features are also observed due to monodentate formate on Cu (m-HCOO–Cu) at 1365 and 1574 cm^{-1} (13, 15, 16). At 423 K, all previously mentioned features are still present. The m-HCOO–Cu features have increased dramatically in intensity and are stable upon purging in He. A doublet centered at 2349 cm^{-1} and a band at ~2110 cm^{-1} are also observed at 423 K, indicating the presence of gas-phase CO_2 and CO absorbed on Cu (CO–Cu) (25), respectively.

At 473 K in flowing methanol, evidence for m-HCOO–Cu is minimal, but a strong peak at 1350 cm^{-1} has developed, which, along with features at 1542, 2693, 2851, and 2928 cm^{-1}, correspond to bidentate formate on Cu (b-HCOO–Cu) (13, 14, 16, 26). Features are also seen at 1715 and 1660 cm^{-1}, which correspond to methyl formate adsorbed on SiO_2 (CH_3OCHO–Si) and Cu (CH_3OCHO–Cu), respectively (15, 23). Also, the features due to adsorbed CO–Cu and gas-phase CO_2 have increased in intensity. Upon purging in He at 473 K, CH_3O–Cu is removed completely, as noted by the disappearance of the bands at 2926, 2894, 2816, and 1442 cm^{-1}. The intense b-HCOO–Cu features are also removed upon purging in He at 473 K. At 523 K in flowing methanol, the intensity of the band for adsorbed CO increases further, and gas-phase CO_2 formation continues. The maximum observed at 2185 cm^{-1} is most likely due to the *R* branch in the spectrum of gas-phase CO. At 523 K there is little evidence for any surface species other than CH_3O–Si, CO–Cu, POM, and a small amount of b-HCOO–Cu. At all temperatures, the intensities of the CH_3O–Cu and b-HCOO–Cu features are always higher during methanol flow, while for m-HCOO–Cu the peak intensity is somewhat higher during purging in He. The features observed for gas-phase CO_2 and CO–Cu between 423 and 523 K are not observable after purging in He.

Figure 2 shows how the infrared absorbances from Fig. 1 for CH_3O–Cu, m-HCOO–Cu, b-HCOO–Cu, CO–Cu, and

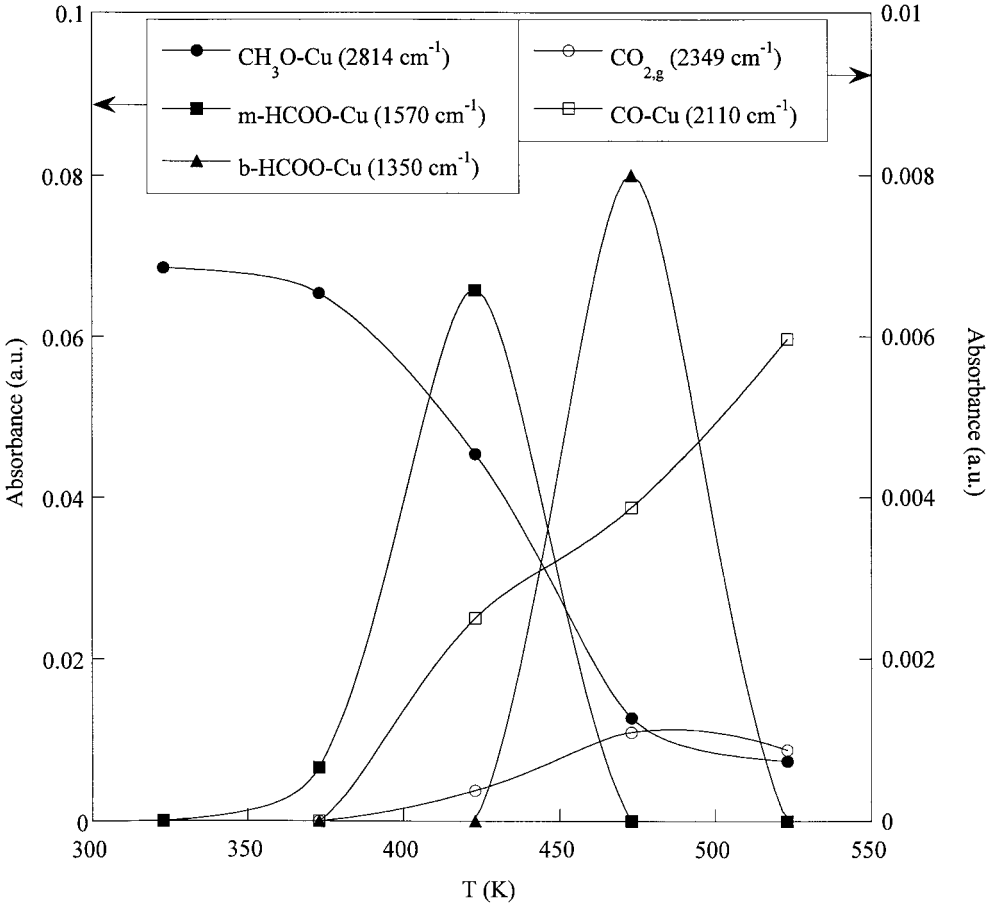

FIG. 2. Absorbance intensities taken from the spectra in Fig. 1 during methanol flow.

gas-phase CO_2 vary as a function of temperature during methanol flow. The intensity of the feature for CH_3O–Cu is highest at 323 K and decreases at higher temperatures. Evidence for m-HCOO–Cu appears at 373 K, whereas b-HCOO–Cu is evident above 423 K. Both formate species exhibit a maximum in surface concentration with increasing temperature. For m-HCOO–Cu this maximum occurs at 423 K, at which point the surface concentration of CH_3O–Cu is changing most rapidly with temperature. The evolution of gas-phase CO_2 and the formation of CO–Cu occur above 373 K. A broad maximum in the intensity of the absorbance for CO_2 occurs at 473 K, coinciding with the maximum in the intensity of the band for b-HCOO–Cu.

ZrO_2/SiO_2. Figure 3 shows infrared spectra taken 30 min after ZrO_2/SiO_2 was exposed to a stream of 1% methanol in Ar at temperatures between 323 and 523 K and 1 atm total pressure. Also shown are spectra taken after purging the catalyst in He for 30 min at each temperature. All bands are more intense during methanol flow than after purging in He. At 323 K features assigned to methoxide on zirconia (CH_3O–Zr) are observed at 2939, 2840, and 1449 cm^{-1} (13, 14, 21, 27–31). Bands due to CH_3O–Si are also observed at 2990, 2956, 2856, 1456 cm^{-1}, and a shoulder at 1620 cm^{-1} due to adsorbed water on silica (H_2O–Si) (13, 32) is also seen. In addition, there is a band at 1592 cm^{-1} due to the Zr–H stretch of dissociatively adsorbed methanol on zirconia in the form CH_3O–Zr–H (33). Other possible assignments for this band include gas-phase H_2O and H_2O adsorbed on zirconia. Neither of these assignments is likely, though, since the band at 1592 cm^{-1} remains strong during He purge, and H_2O adsorbed on zirconia results in a band near 1635 cm^{-1} (21). In the OH stretching region, negative peaks appear at 3743 and 3670 cm^{-1}, corresponding to hydroxyl groups on silica (HO–Si) (13, 24) and bridging hydroxyl groups on zirconia (HO–Zr) (13, 29, 34, 35), respectively. Since the spectra are referenced to the reduced catalyst under He flow at the temperature of interest, the appearance of negative bands demonstrates that OH groups are consumed upon adsorption.

As the temperature is increased, no additional surface species are observed to form on ZrO_2/SiO_2 during methanol adsorption or upon subsequent purging in He. Negative bands at 1567, 1381, and 1368 cm^{-1}, which are characteristic of bidentate formate on zirconia (b-HCOO–Zr) (13, 14, 18, 21, 27–31, 34, 36), appear as the temperature is increased. This indicates that there was a small amount of residual b-HCOO–Zr present on the catalyst prior to methanol adsorption, even though the sample was reduced for 2 days in H_2 at 523 K. The loss in the residual formate species may be due to reaction with water and/or atomic hydrogen resulting from the dissociative adsorption of methanol. This later reaction may not occur as readily during reduction in hydrogen, as zirconia is not effective for the dissociative adsorption of hydrogen (37).

Figure 4 shows the effect of temperature on the intensities of the peaks for CH_3O–Zr and HO–Zr taken from Fig. 3 during the flow of methanol. Since the bands for HO–Zr are negative (see Fig. 3), the values shown in Fig. 4 represent hydroxyl group consumption resulting from methanol exposure. The methoxide features is most intense when the hydroxyl group consumption is high (323 K), and the intensities of both features decrease as the temperature is increased. It is evident from Fig. 4 that the decrease in the surface concentration of CH_3O–Zr at elevated temperatures is closely correlated with a decrease in the consumption of HO–Zr groups.

Figure 5 shows infrared spectra obtained during continued purging in He of ZrO_2/SiO_2 at 523 K for an additional 125 h following the exposure described in Fig. 3. After about 25 h, features emerge at 1560, 1388, 1370 cm^{-1} due to b-HCOO–Zr, while features due to CH_3O–Zr at 2943 and 2844 cm^{-1} decrease significantly in intensity. At longer times the features for b-HCOO–Zr continue to increase in intensity, while the features for CH_3O–Zr continue to decrease. The peaks due to CH_3O–Si also decrease with increasing time, but are more persistent than those for CH_3O–Zr. The formation of monodentate carbonate on zirconia (m-CO_3–Zr) is indicated by the weak band at 1483 cm^{-1} (13, 14, 21, 30, 34, 38–40). A companion feature which should appear at ~1385 cm^{-1} is obscured by the b-HCOO–Zr bands. Figure 5 also illustrates the behavior of HO–Si and HO–Zr species during continued purge in He. With increasing time in He the negative bands for these species become less intense, indicating an increase in the surface concentration of HO–Si and HO–Zr.

Figure 6 shows the effect of time on the peak intensities for CH_3O–Zr, b-HCOO–Zr, and HO–Zr species taken from Fig. 5 during He purging at 523 K. It is evident that as the methoxide band intensities decrease, the formate band intensities increase, and the intensity of the HO–Zr band is partially recovered.

$Cu/ZrO_2/SiO_2$. Figure 7 shows infrared spectra taken 30 min after $Cu/ZrO_2/SiO_2$ was exposed to a stream of 1% methanol in Ar at temperatures between 323 and 523 K and 1 atm total pressure. Also shown are spectra taken after purging the catalyst in He for 30 min at each temperature. All features except those for b-HCOO–Zr (see below) are more intense during methanol flow than after purging in He. At 323 K features assigned to CH_3O–Zr are observed at 2933, 2830, and 1450 cm^{-1}. Bands due to CH_3O–Si are also observed at 2988, 2952, 2848, and 1464 cm^{-1}. A band due to the Zr–H stretch of methanol dissociatively adsorbed on zirconia in the form CH_3O–Zr–H is observed at 1592 cm^{-1}, as well as a band due to H_2O–Si, as evidenced by the feature at 1622 cm^{-1}.

At 373 K during He purge, features due to b-HCOO–Zr become apparent at 1577, 1386, and 1368 cm^{-1}. These features reach a maximum in intensity at 423 K and are always

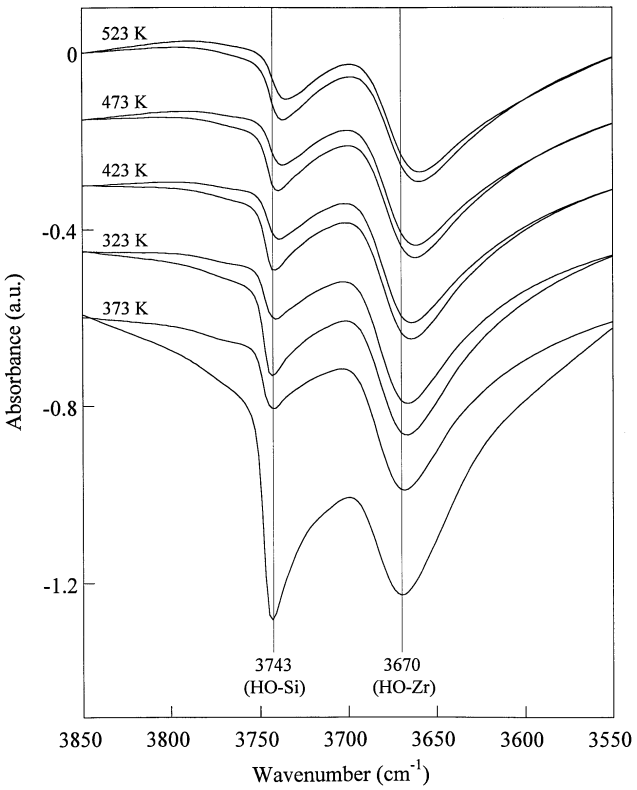

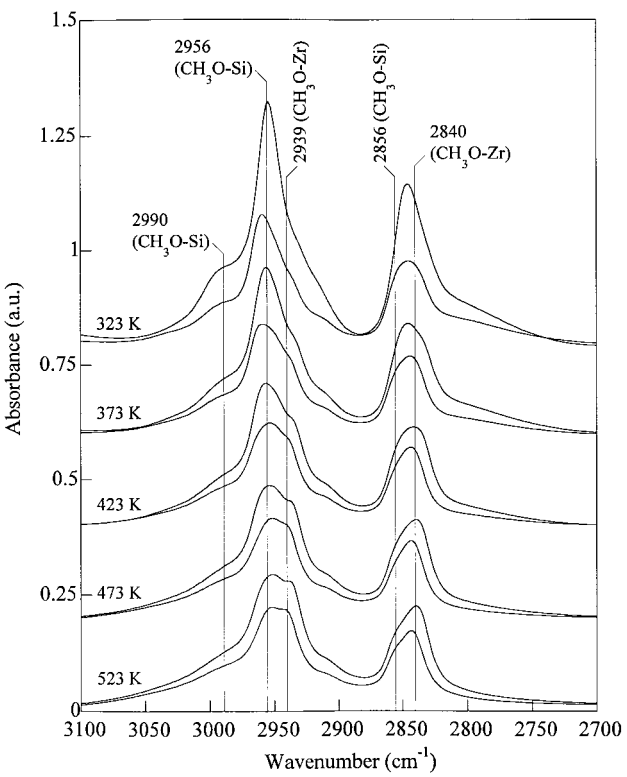

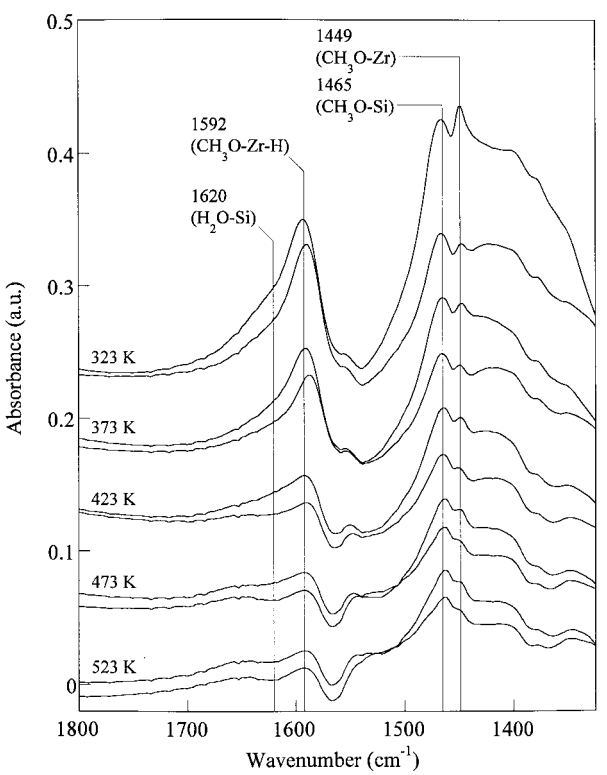

FIG. 3. Infrared spectra taken during exposure of ZrO_2/SiO_2 to a stream of 1% methanol in Ar flowing at 60 cm^3/min for 30 min at atmospheric pressure (top spectrum at each temperature in the regions 3100–2700 cm^{-1} and 1800–1300 cm^{-1}, and bottom spectrum at each temperature in the region 3850–3550 cm^{-1}), and after exposure to He flowing at 60 cm^3/min for 30 min at atmospheric pressure (bottom spectrum at each temperature in the regions 3100–2700 cm^{-1} and 1800–1300 cm^{-1}, and top spectrum at each temperature in the region 3850–3550 cm^{-1}). Spectra referenced to reduced ZrO_2/SiO_2 under atmospheric pressure He flow at each temperature.

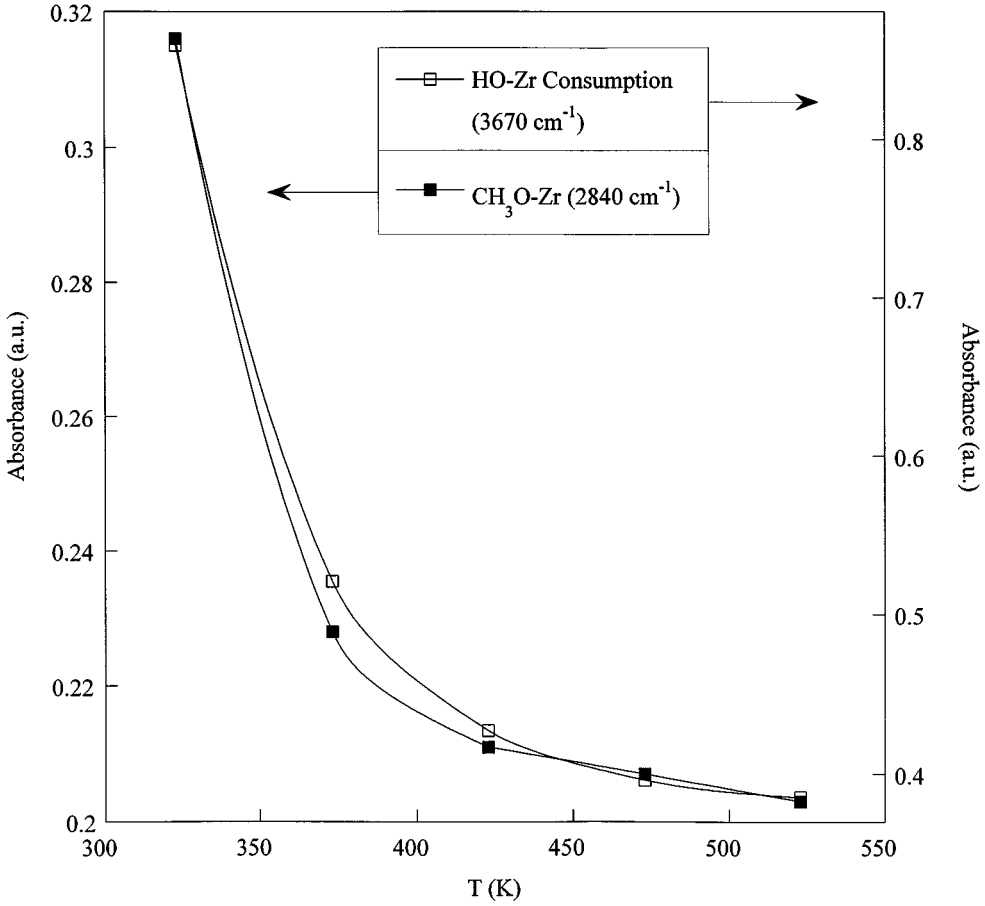

FIG. 4. Absorbance intensities taken from the spectra in Fig. 3 during methanol flow.

stronger during purge in He than under methanol flow at any temperature. A band for CO–Cu (2119 cm^{-1}) (25), as well as a doublet for gas-phase CO_2 (centered at 2349 cm^{-1}), become evident at 423 K. These features are observed only during methanol flow and are not observed after purging in He at any temperature. The feature for gas-phase CO_2 increases in intensity at higher temperatures, while the feature due to CO–Cu reaches a maximum in intensity at 473 K. There is also a band observed at 2307 cm^{-1}, which is probably due to CO_2 weakly adsorbed on zirconia, as this feature was not observed on Cu/SiO_2. At 473 K, a weak band associated with b-HCOO–Cu is present at 1350 cm^{-1}, and at 473 and 523 K, the presence of methyl formate on Cu is indicated by the band at 1666 cm^{-1}. In the OH stretching region, negative peaks appear at 3740 cm^{-1} (HO–Si) and 3670 cm^{-1} (HO–Zr), indicating the consumption of OH groups, which is at a maximum at 323 K and decreases at higher temperatures.

Figure 8 shows the peak intensities for CH_3O–Zr, b-HCOO–Zr, HO–Zr, CO–Cu, and gas-phase CO_2 as a function of temperature, taken from Fig. 7 during the flow of methanol. The intensity of the methoxide peak is relatively constant up to 423 K and then increases slightly at higher temperatures. The hydroxyl group consumption is at a maximum at 323 K and decreases at higher temperatures. Formate formation is observed at 373 K and the formate surface concentration goes through a maximum at 423 K, at which temperature gas-phase CO_2 and CO–Cu formation become observable.

Temperature Programmed Desorption and Reaction of Methanol

Figure 9 shows the TPD spectrum obtained following the adsorption of methanol on Cu/SiO_2 at room temperature. The gas-phase products observed are CH_3OH, CH_2O, CO_2, H_2, and H_2O. Methanol desorbs in a single relatively sharp band exhibiting a maximum at 359 K ($T_m = 359$ K), while formaldehyde desorbs at a slightly higher temperature ($T_m = 379$ K). Carbon dioxide formation is observed above ~375 K and the desorption spectrum exhibits maxima at 452 and 484 K. These maxima occur at the temperatures at which m-HCOO–Cu and b-HCOO–Cu species exhibit maximal decreases in surface concentration with

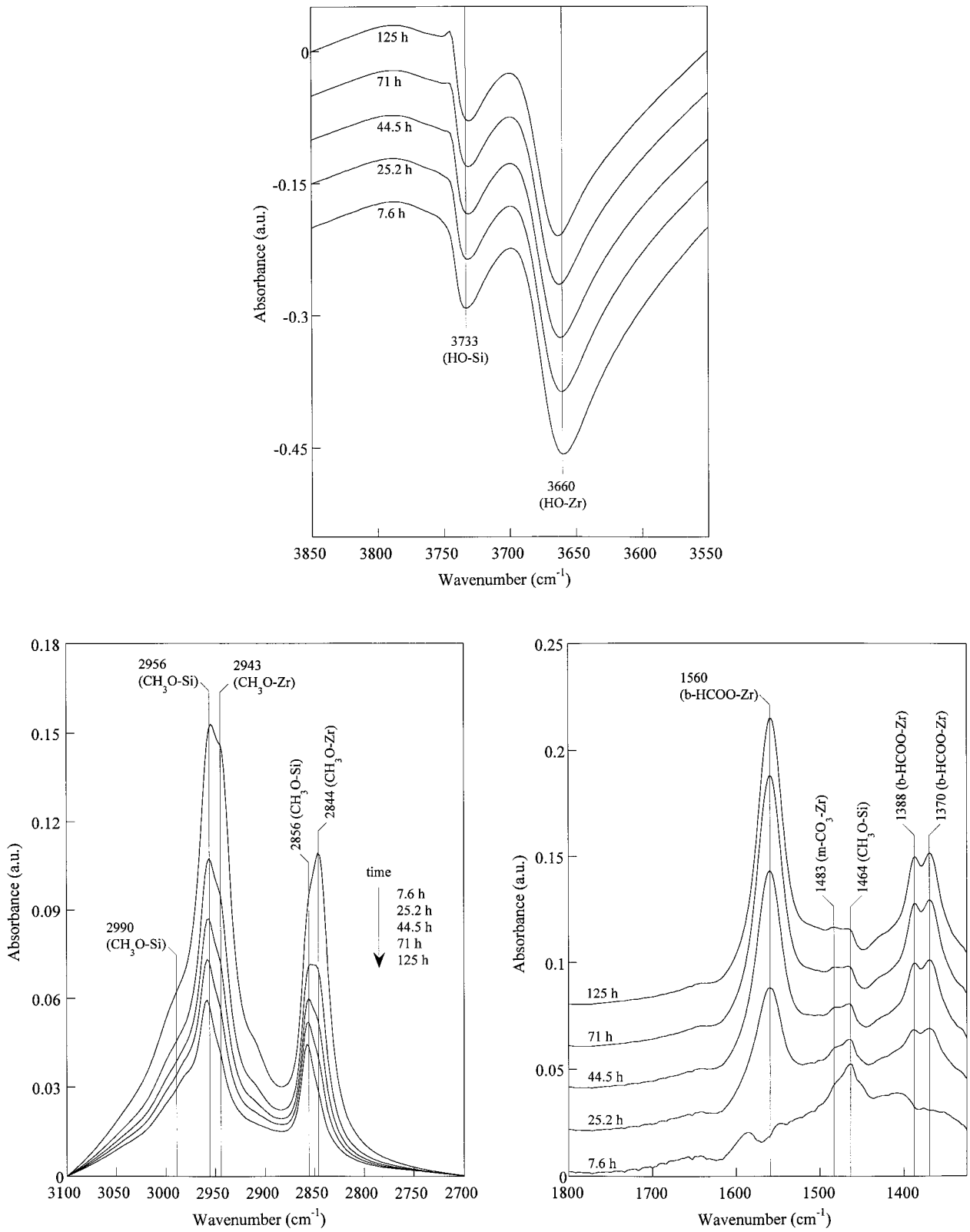

FIG. 5. Infrared spectra taken for ZrO_2/SiO_2 at 523 K during continued purging in He at a rate of 60 cm^3/min. Spectra referenced to reduced ZrO_2/SiO_2 under atmospheric pressure He flow at 523 K.

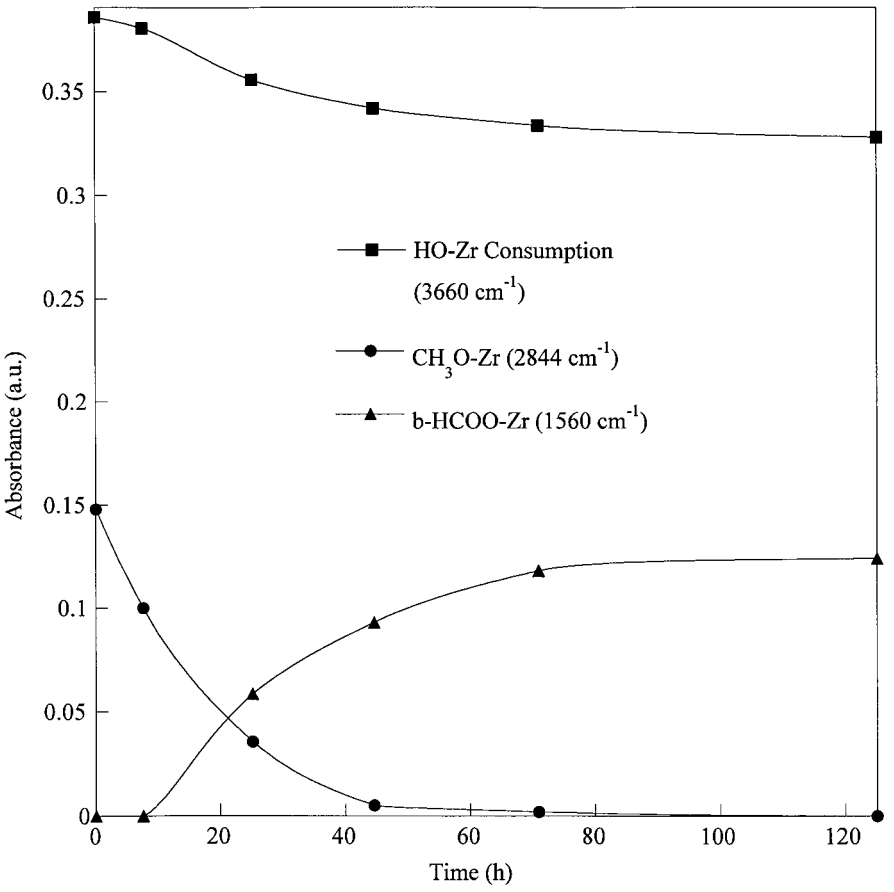

FIG. 6. Absorbance intensities taken from the spectra in Fig. 5.

temperature (see Fig. 2). Hydrogen is evolved concurrently with CH_2O and CO_2. Water exhibits a maximum at 368 K, and a second increase in water formation is observed above 470 K.

The results obtained during the TPD of methanol on $Cu/ZrO_2/SiO_2$ following methanol adsorption at room temperature are shown in Fig. 10. The species formed are the same as for Cu/SiO_2, but the maxima observed occur at higher temperatures. In this case, CO_2 is observed to desorb in a single peak exhibiting a maximum at 495 K, at which temperature the decrease in the surface concentration with temperature of b-HCOO–Zr species is also at a maximum (see Fig. 8). Table 1 summarizes the quantity of material desorbed and the temperature of the peak maximum for each species observed in the TPD spectra shown in Figs. 9 and 10.

Figure 11 shows the results obtained during the TPR of methanol for Cu/SiO_2. The gas-phase products observed are CH_2O, CO_2, CO, CH_3OCH_3, CH_3OCHO, H_2, and H_2O. Water is formed at low temperatures, and formaldehyde is observed above ~340 K. Significant H_2, CO, and CO_2 formation is observed above ~400 K, and methyl formate is observed above ~430 K. A small quantity of dimethyl ether is also formed above ~460 K. The results obtained during the TPR of methanol on $Cu/ZrO_2/SiO_2$ are shown in Fig. 12. The gas-phase products observed are the same as for Cu/SiO_2, but the concentrations observed are different. The threshold temperatures for product formation are similar to those observed for Cu/SiO_2, with the exception of methyl formate which is observed only above ~460 K on $Cu/ZrO_2/SiO_2$. For the TPD and TPR spectra shown in

TABLE 1

Quantities of Species Formed and Temperatures of Peak Maxima Observed during the TPD of Methanol for the Results Shown in Figs. 9 and 10

	Catalyst			
	Cu/SiO_2		$Cu/ZrO_2/SiO_2$	
Species	T_m (K)	Quantity formed (μmol/g)	T_m (K)	Quantity formed (μmol/g)
H_2	452, 491	32.2	495	170
H_2O	368	51.6	423	160
CO_2	452, 484	20.9	495	36.8
CH_2O	379	2.8[a]	412	17.5[a]
CH_3OH	359	312	367	1380

[a] Not quantified.

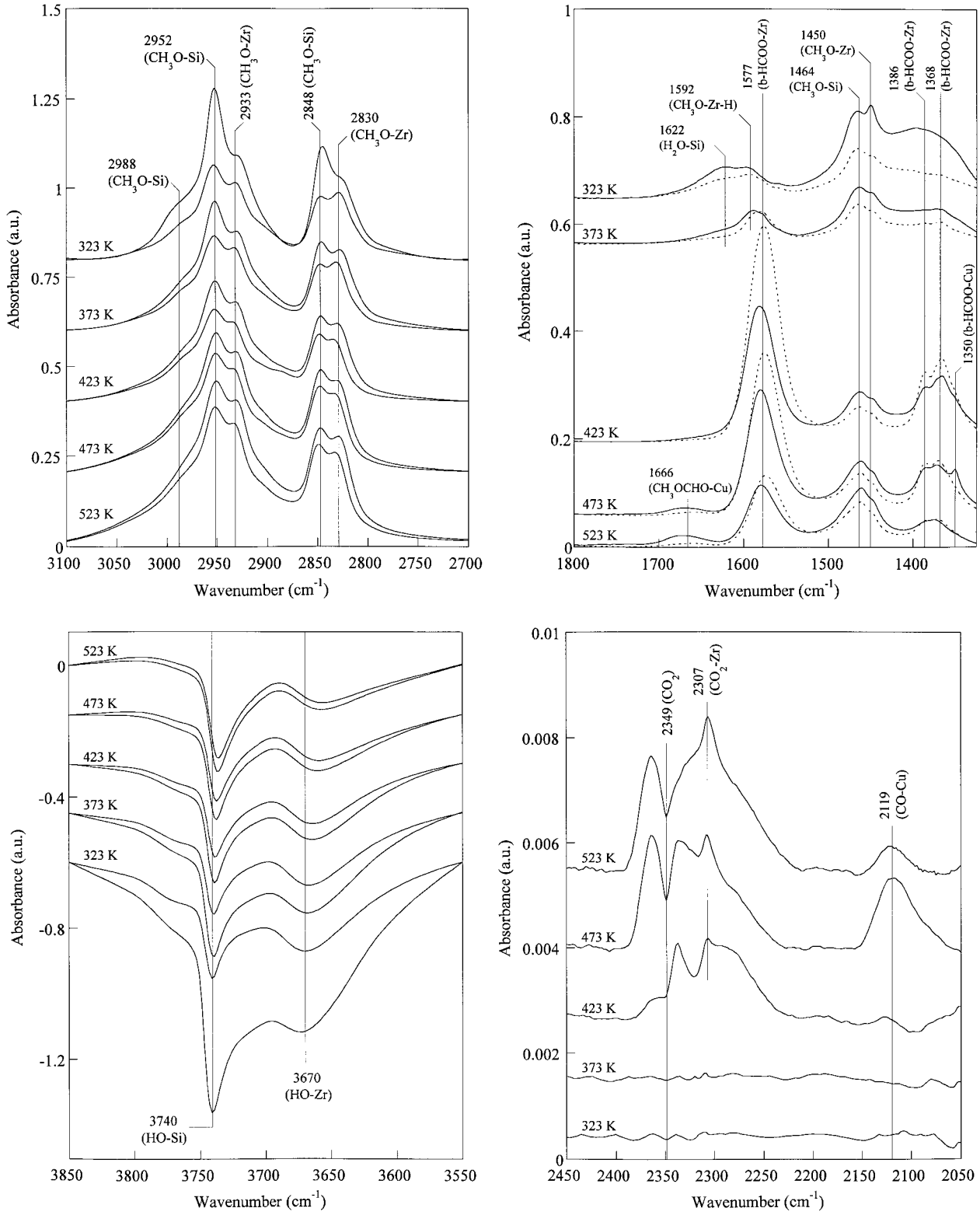

FIG. 7. Infrared spectra taken during exposure of $Cu/ZrO_2/SiO_2$ to a stream of 1% methanol in Ar flowing at 60 cm^3/min for 30 min at atmospheric pressure (top spectrum at each temperature in the region 3100–2700 cm^{-1}, solid spectrum at each temperature in the region 1800–1300 cm^{-1}, and bottom spectrum at each temperature in the region 3850–3550 cm^{-1}) and after exposure to He flowing at 60 cm^3/min for 30 min at atmospheric pressure (bottom spectrum at each temperature in the region 3100–2700 cm^{-1}, dotted spectrum at each temperature in the region 1800–1300 cm^{-1}, and top spectrum at each temperature in the region 3850–3550 cm^{-1}). In the region 2450–2050 cm^{-1}, only spectra taken during methanol exposure are shown. Spectra referenced to reduced $Cu/ZrO_2/SiO_2$ under atmospheric pressure He flow at each temperature.

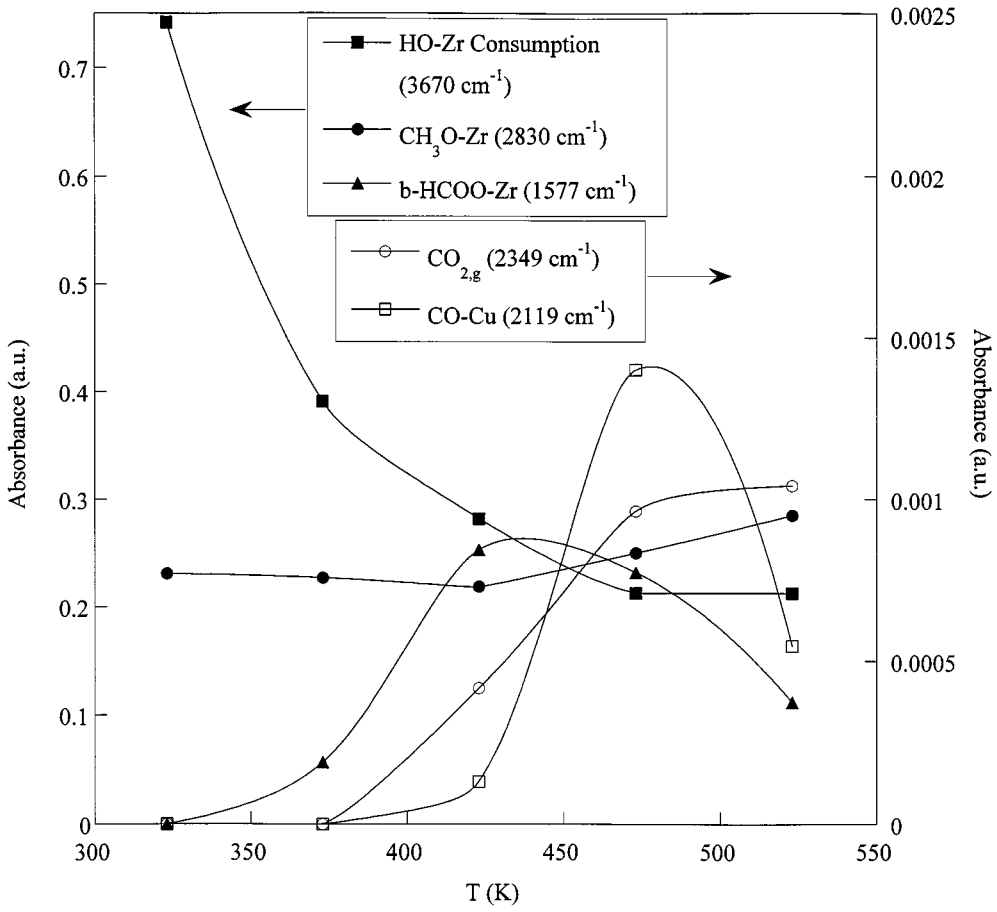

FIG. 8. Absorbance intensities taken from the spectra in Fig. 7 during methanol flow.

Figs. 9–12, the concentrations of CH_2O, CH_3OCHO, and CH_3OCH_3 are not quantified.

DISCUSSION

Previous studies have demonstrated that methanol interacts very weakly on clean Cu(100) (41), Cu(110) (42, 43), and Cu(111) (44) surfaces and that the presence of surface oxygen is required for methanol decomposition to proceed efficiently on these surfaces. In the present study the decomposition of methanol over Cu/SiO_2 proceeds readily and results in CO_2 formation above ~390 K, which requires a source of oxygen to occur. Prior to discussing the means by which decomposition products are formed, it is therefore important to consider the possible sources of oxygen. Previous studies on methanol decomposition over $Cu/ZnAl_2O_4$ reduced in H_2 at 523 K (45), on $Cu/ZnO/Al_2O_3$ reduced in H_2 at 520 K (46), and on Cu/SiO_2 reduced in H_2 at 623 K (15) have suggested that oxygen remains on the surface of Cu as a consequence of incomplete reduction. Although it is likely that in the present work a small but finite amount of oxygen remains on the Cu surface of the Cu/SiO_2 catalyst after reduction in H_2 at 523 K for >8 h, it cannot be responsible for generating the amount of CO_2 observed based upon the following argument. The Cu/SiO_2 catalyst used in this study has a Cu surface area of 1.36 m^2/g-cat, which corresponds to 33.0 μmol Cu/g-cat, using a Cu surface density of 1.46×10^{19} Cu atoms/m^2 (47). Table 1 indicates that 20.9 μmol CO_2/g-cat are formed during the TPD of methanol. For residual oxygen on Cu to be incorporated into the CO_2 evolved requires that 20.9 μmol CuO/g-cat be present on the catalyst surface or that 63.3% of the Cu surface be CuO following reduction in H_2. This seems extremely unlikely, since it was observed that during temperature programmed reduction of Cu/SiO_2 prepared by the same technique as used in the present study, hydrogen consumption ceased by 470 K (48). Another source of oxygen is the reactor feed. Mass spectrometric analysis of the 1.0% UHP methanol in argon used in this study shows the presence of 300 ppm (0.012 μmol/cm^3) H_2O. The dissociation of water to hydrogen and adsorbed oxygen has been observed to occur at 346 K on reduced polycrystalline Cu (49) and has been reported to be promoted by adsorbed oxygen (50, 51). It is therefore proposed that the water present in the

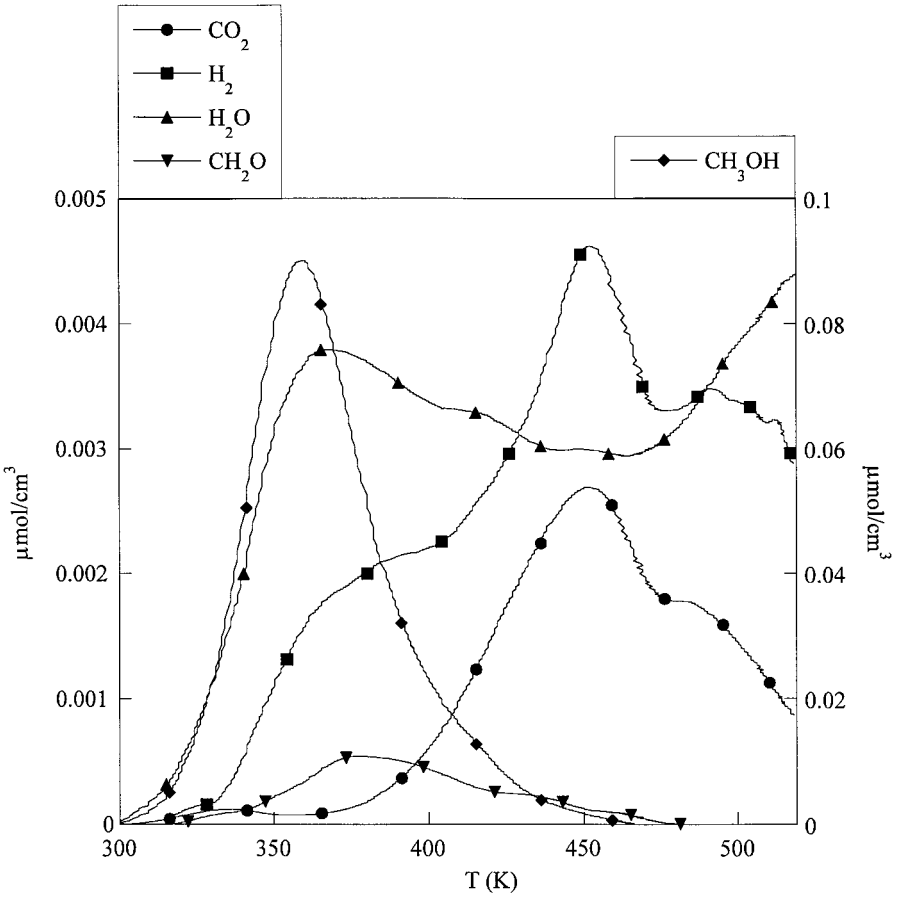

FIG. 9. TPD spectrum obtained after exposure of reduced Cu/SiO_2 to 1% methanol in Ar flowing at 60 cm^3/min for 30 min at 300 K and subsequent purging in He flowing at 60 cm^3/min for 1 h at 300 K. The heating rate is 4 K/min and the carrier gas is He flowing at 60 cm^3/min.

feed gas dissociates on Cu to provide the oxygen required for the formation of CO_2.

The carbon containing products observed during the reaction of methanol with Cu/SiO_2 are formaldehyde, which formed above 340 K, CO_2, formed above 390 K, CO, formed above 410 K, methyl formate, formed above 430 K, and a small amount of dimethyl ether, formed above 440 K. The reaction by which formaldehyde is formed in the gas phase is proposed to be (42, 52)

$$2CH_3OH + O_{(a)} \rightarrow 2H_2CO + H_2O + H_2. \quad [1]$$

The TPD spectrum in Fig. 9 shows that H_2, H_2O, and CH_2O evolve simultaneously, providing support for the above reaction. Reaction [1] is favored over the dehydrogenation of methanol to formaldehyde and hydrogen in the presence of adsorbed oxygen (42). In reaction [1] water is formed by the interaction of methanol with adsorbed oxygen on Cu:

$$2CH_3OH + O_{(a)} \rightarrow 2CH_3O_{(a)} + H_2O. \quad [2]$$

Hydrogen and formaldehyde are formed by the dehydrogenation of methoxide species:

$$2CH_3O_{(a)} \rightarrow 2CH_2O + H_2. \quad [3]$$

Methoxide species are observed to form readily on Cu following the exposure of Cu/SiO_2 to methanol at 323 K (see Fig. 1), and reaction [2] has been reported to be the dominant route for methanol adsorption on Cu surfaces (42, 43, 52). Direct evidence for adsorbed formaldehyde was not observed. However, above 323 K POM is observed on the catalyst surface (see Fig. 1), which continues to accumulate at higher temperatures. The presence of POM provides indirect evidence for the formation of formaldehyde, as POM is formed via the polymerization of formaldehyde (23). Direct evidence for gas-phase formaldehyde formation is observed during TPD and TPR of methanol (see Figs. 9 and 10). Reaction [3] has been proposed to be responsible for formaldehyde formation from methoxide species on Cu surfaces (15, 16, 42, 53).

CO_2 formation observed above 390 K is proposed to arise via the following the reaction:

$$CH_3OH + O_{(a)} \rightarrow CO_2 + 2H_2. \quad [4]$$

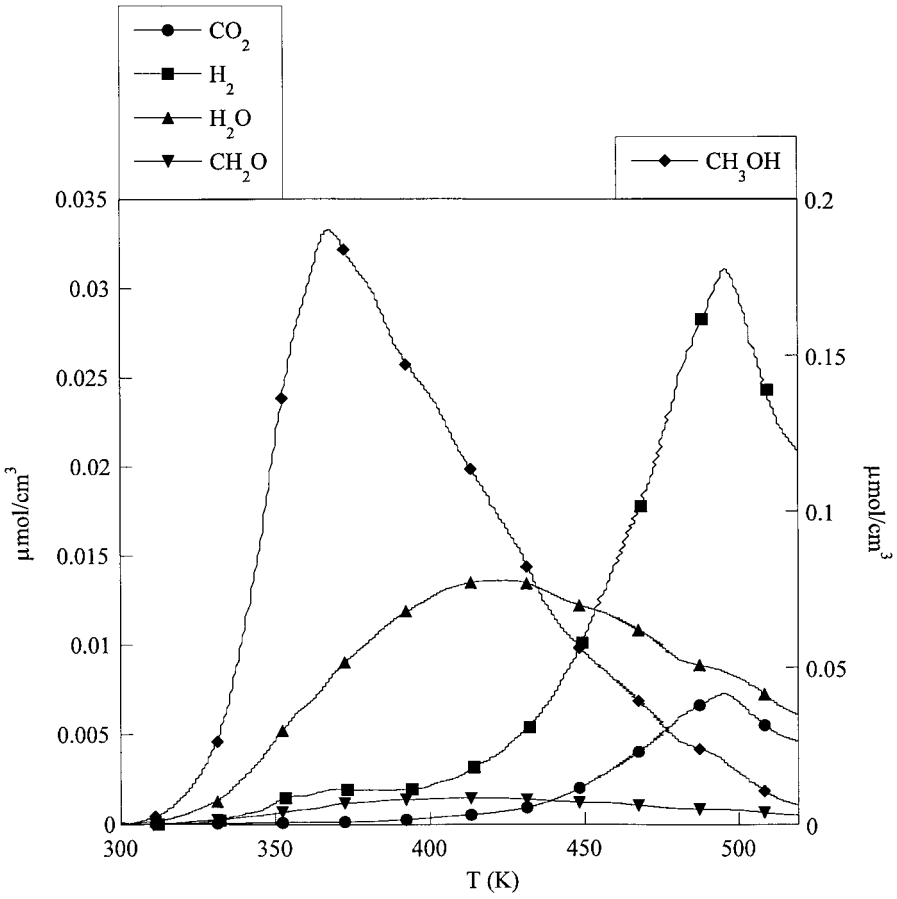

FIG. 10. TPD spectrum obtained after exposure of reduced $Cu/ZrO_2/SiO_2$ to 1% methanol in Ar flowing at 60 cm^3/min for 30 min at 300 K and subsequent purging in He flowing at 60 cm^3/min for 1 h at 300 K. The heating rate is 4 K/min and the carrier gas is He flowing at 60 cm^3/min.

The surface oxygen is provided by the dissociation of water present in the feed. Hence reaction [4] can alternatively be written as the steam reforming of methanol:

$$CH_3OH + H_2O \rightarrow CO_2 + 3H_2. \qquad [5]$$

Carbon dioxide and hydrogen are formed by the decomposition of formate species on Cu (15, 16, 42, 43, 54–56). The spectra shown in Fig. 1 reveal that m-HCOO–Cu is formed at 373 K. The concentration of m-HCOO–Cu reaches a maximum value at 423 K, at which point the decrease in the CH_3O–Cu surface concentration with temperature is also at a maximum (see Fig. 2). These results suggests that Cu methoxide undergoes oxidation to m-HCOO–Cu. The precursor to m-HCOO–Cu is proposed to be adsorbed formaldehyde (15, 16), the formation of which occurs as described above. The source of oxygen required for the oxidation of CH_2O–Cu to m-HCOO–Cu is provided by the dissociation of water present in the feed. During methanol exposure, formate species have been observed on Cu/SiO_2 (15, 16) and have been proposed to form on Cu single crystals (42, 44). The formation of these species has been attributed to the reaction of adsorbed formaldehyde with oxygen on Cu (15, 16, 42, 43). Methylenebisoxy species have been proposed as intermediates in this reaction (16).

The decomposition of m-HCOO–Cu to CO_2 and H_2 is supported by the observation of gas-phase CO_2 above 373 K in the infrared spectra presented in Fig. 1, as well as the significant CO_2 and H_2 formation observed above 390 K during the TPR of methanol (see Fig. 11). The formation of adsorbed CO–Cu at 423 K and above (see Fig. 1) and CO in the gas phase above 410 K (see Fig. 11) is primarily attributed to the decomposition of methyl formate (see below). CO may also form via the dissociation of CO_2, the extent of which has been measured to be ~20% on Cu/SiO_2 (57). As the gas-phase CO concentration observed above 410 K (see Fig. 11) is comparable to, or greater than, the measured gas-phase CO_2 concentration, this route for CO formation must be considered secondary.

At 473 K, features for m-HCOO–Cu have disappeared while features for b-HCOO–Cu have appeared in the spectra presented in Fig. 1. It is probable that m-HCOO–Cu is converted to b-HCOO–Cu near this temperature. The

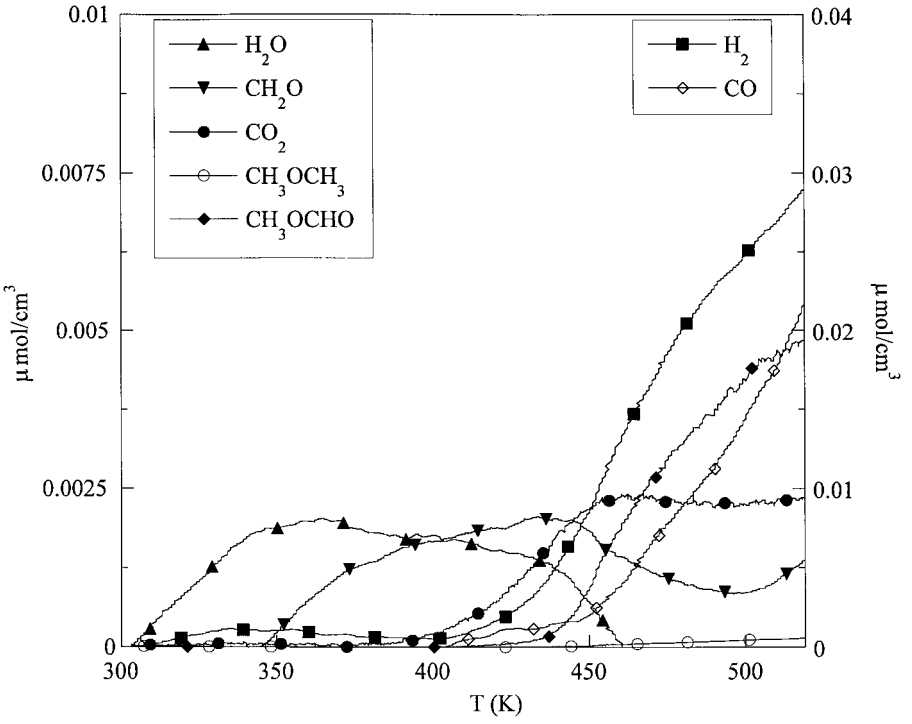

FIG. 11. TPR spectrum obtained after exposure of reduced Cu/SiO_2 to 1% methanol in Ar flowing at 60 cm^3/min for 30 min at 300 K and subsequently heating the sample at 4 K/min while flowing 1% methanol in Ar at 60 cm^3/min.

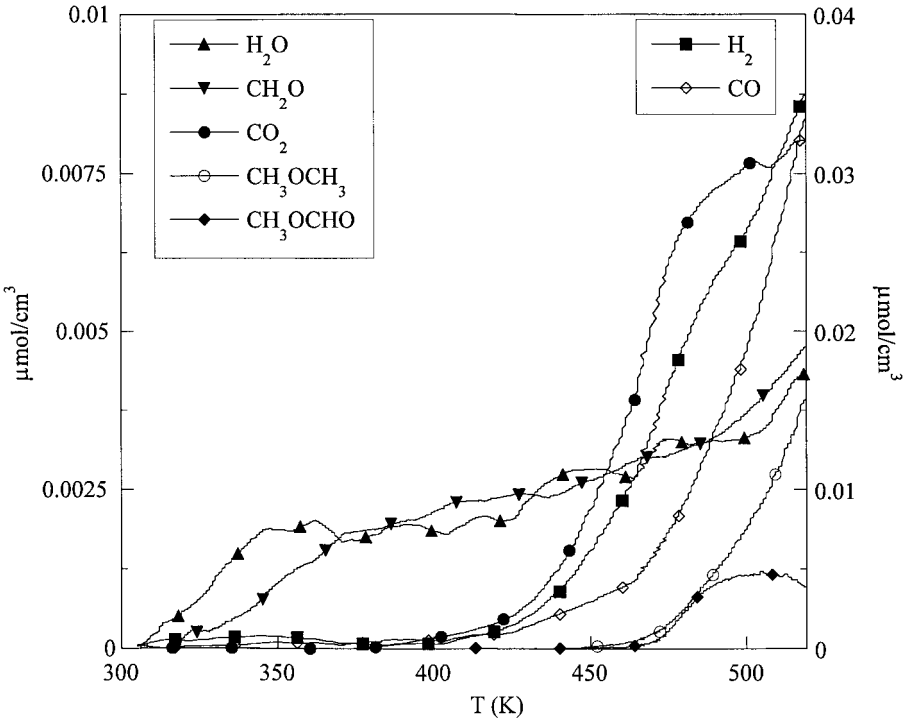

FIG. 12. TPR spectrum obtained after exposure of reduced $Cu/ZrO_2/SiO_2$ to 1% methanol in Ar flowing at 60 cm^3/min for 30 min at 300 K and subsequently heating the sample at 4 K/min while flowing 1% methanol in Ar at 60 cm^3/min.

preferential formation of m-HCOO–Cu over b-HCOO–Cu has been reported previously during methanol decomposition on oxidized Cu/SiO_2 (15, 16). As m-HCOO–Cu is absent from the catalyst surface at 473 K, the continued generation of CO_2 observed in the infrared spectrum shown in Fig. 1, as well as the H_2 and CO_2 generation observed in the TPD and TPR spectra (see Figs. 9 and 11), is attributed to the decomposition of b-HCOO–Cu. The decomposition of both m-HCOO–Cu and b-HCOO–Cu to CO_2 and H_2 is clearly seen in the TPD spectra shown in Fig. 9, where two desorption maxima are observed for CO_2 and H_2 at the temperatures where the decrease in m-HCOO–Cu and b-HCOO–Cu surface concentrations with temperature are at a maximum (see Fig. 2).

The formation of methyl formate is also indicated at 473 K in the infrared spectra presented in Fig. 1 and beginning at ~430 K during the TPR of methanol (Fig. 11), as has been observed previously during the decomposition of methanol on Cu/SiO_2 (15, 23). It is proposed that methyl formate is formed by

$$2CH_3OH + O_{(a)} \rightarrow CH_3OCHO + H_2O + H_2, \quad [6]$$

which can be written to include the dissociation of water as

$$2CH_3OH \rightarrow CH_3OCHO + 2H_2. \quad [7]$$

It has been suggested that methyl formate is formed via the interaction of adsorbed methoxide and formaldehyde species (15, 58), the formation of which has been described above.

The formation of CO observed above ~410 K is attributed to the decomposition of methyl formate which can proceed via the following two reactions depending on the catalyst (59):

$$CH_3OCHO \rightarrow 2CO + 2H_2 \quad [8]$$

$$CH_3OCHO \rightarrow CO + CH_3OH. \quad [9]$$

Both reaction [8] (15) and reaction [9] (23) have been observed over Cu/SiO_2, and the decomposition of methyl formate to CO and H_2 has been observed to occur quite readily on Cu/SiO_2 at 503 K (23) and 538 K (15). The TPR spectra shown in Fig. 11 indicate significant H_2 and CO formation above 410 K, which is attributed to the decomposition of methyl formate. It appears that reaction [8] is the dominant route for methyl formate decomposition under the conditions of the current investigation, while reaction [9] also occurs at temperatures above 500 K as discussed below. It is also likely that much of the adsorbed CO on Cu observed at 473 K during the present study is due to the decomposition of methyl formate. The small amount of dimethyl ether observed to form above 440 K is attributed to the dehydration of methanol.

Based upon the cumulative evidence discussed above, a proposed mechanism for methanol decomposition on the Cu surface of the Cu/SiO_2 catalyst is presented in Fig. 13. Methanol reacts with surface oxygen to form methoxide species on Cu and water (42, 43, 52). Dehydrogenation of methoxide on Cu results in the formation of adsorbed formaldehyde on Cu (15, 16, 42, 52, 53). Adsorbed formaldehyde can react with surface oxygen to form methylenebisoxy (16), desorb into the gas phase (15, 16, 42, 52, 53), polymerize to form polyoxymethylene (23), or react with methoxide to form methyl formate (15, 58). Methyl formate subsequently desorbs into the gas phase or decomposes to form CO and hydrogen or CO and methanol (15, 23, 59). Dehydrogenation of methylenebisoxy results in the formation of monodentate formate on Cu at 373 K. Bidentate formate on Cu is also present above 423 K. Both types of formate species on Cu decompose to gas-phase CO_2 and hydrogen.

The relative extent of methanol decomposition to CO_2 via the pathway indicated on the left side of Fig. 13 versus the decomposition to CO indicated on the right of Fig. 13 depends upon the reaction conditions. In the absence of gas-phase methanol, only decomposition to CO_2, H_2, and formaldehyde and H_2O formation occur (left side of Fig. 13), as indicated by the TPD spectra shown in Fig. 9. The reaction of CH_3O–Cu with O–Cu to give CO_2 and H_2 yields 3 H atoms per CO_2 molecule (see Fig. 13). One H atom is generated for each CH_3O–Cu group converted to formaldehyde. Table 1 indicates the ratio of H_2/CO_2 formation is 1.54 during the TPD of methanol. This result suggests that of the methoxide species decomposing, 93% form CO_2 and H_2 and 7% form formaldehyde and hydrogen.

In the presence of gas-phase methanol, decomposition to CO as indicated by the right side of Fig. 13, appears to be dominant particularly at higher temperatures. For example at 463 K during TPR the concentration ratio of CO/CO_2 is 2, while at 520 K this ratio is 9.3. Interestingly, approximately the same amount of CO_2 is formed in the presence of gas-phase methanol (TPR) as in the absence of gas-phase methanol (TPD). The decomposition of two CH_3O–Cu groups to CO and H_2 via a methyl formate intermediate would yield 6 H atoms per 2 CO molecules formed, or a H_2/CO ratio of 1.5, while the same decomposition to CO and CH_3OH would yield 2 H atoms per CO molecule formed, or a H_2/CO ratio of 1 (see Fig. 13). Additionally, methanol decomposition to CO_2 and H_2 gives a H_2/CO_2 ratio of 1.5 as described above. Hence, the ratio of $[H_2]/([CO]+[CO_2])$ formed during the TPR of methanol versus temperature should be 1.5 if methoxide species decompose only to CO, CO_2, and H_2, greater than 1.5 if significant quantities of gas-phase formaldehyde and methyl formate are formed, and less than 1.5 if significant quantities of methyl formate are decomposed to CO and methanol.

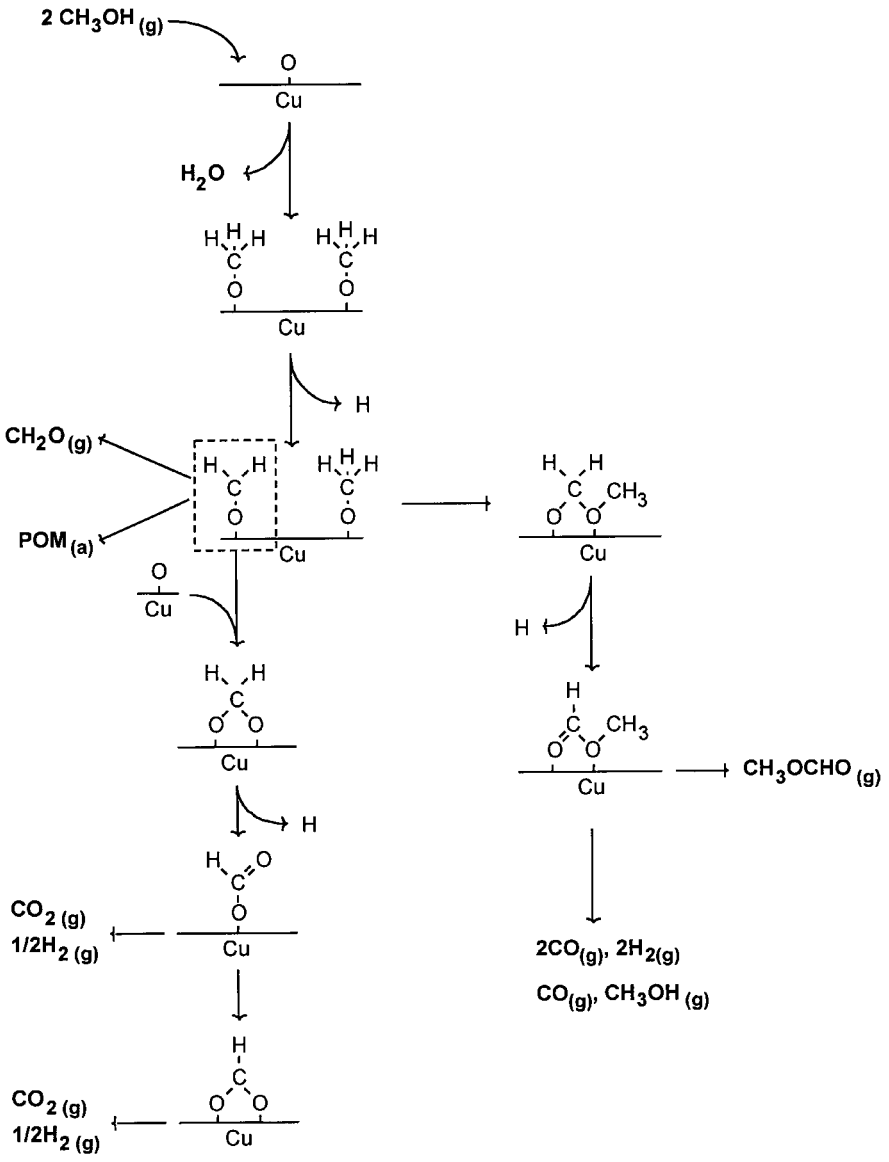

FIG. 13. Proposed mechanism for the decomposition of methanol on Cu/SiO_2.

A plot of the ratio of $[H_2]/([CO]+[CO_2])$ formed during TPR of methanol versus temperature is given in Fig. 14. At 430 K methyl formate formation is not observed, and the ratio is 1.5, indicating that during the TPR of methanol, formaldehyde is not formed in significant quantities, even though the gas-phase formaldehyde concentration is at a maximum at this temperature. The ratio increases to ~2.2 at 447–462 K. At 450 K the concentration of CO plus CO_2 is 0.004 μmol/cm^3. A ratio of 1.5 would result in a H_2 concentration on 0.006 μmol/cm^3. The observed H_2 concentration is 0.009 μmol/cm^3. The additional 0.003 μmol/cm^3 H_2 is accounted for by the formation of methyl formate, which liberates 2 H atoms per methyl formate formed from 2 methoxide groups (see Fig. 13). This suggests that the methyl formate concentration at 450 K is roughly 0.003 μmol/cm^3, indicating that more methanol is converted to methyl formate than CO or CO_2 at 450 K. Above 462 K, the ratio again decreases to 1.5 at 503 K, indicating that methyl formate formation becomes negligible compared to methyl formate decomposition. This can also be observed directly by the sharp rise in CO and H_2 concentration relative to the methyl formate concentration above 460 K seen in Fig. 11. Above 503 K, the ratio falls slightly below 1.5, suggesting that methyl formate decomposition to CO and methanol (reaction (9)) occurs as well. Since the pathway indicated on the right side of Fig. 13 requires reaction between adsorbed formaldehyde and methoxide to give methyl formate above 430 K, it is not surprising that this route does not occur in the absence of gas-phase methanol, as the surface concentrations of formaldehyde and

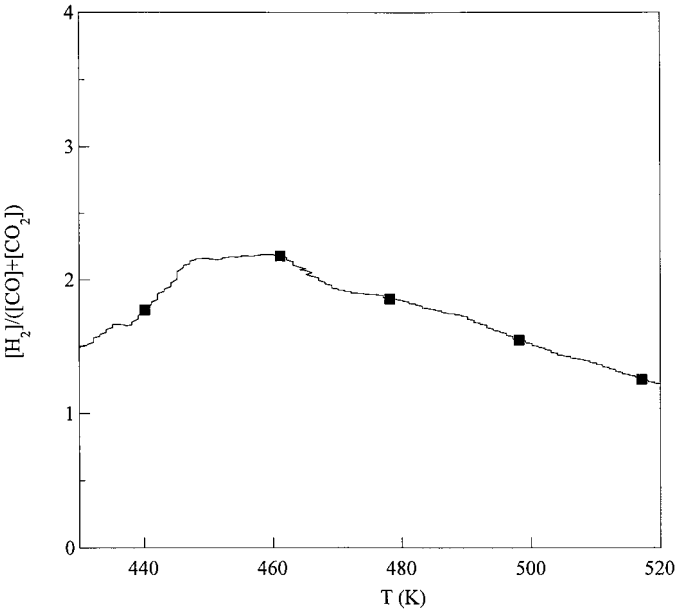

FIG. 14. The ratio of the concentration of hydrogen to the concentration of CO plus CO_2 $[H_2]/([CO]+[CO_2])$ as a function of temperature for the TPR spectrum shown in Fig. 11.

methoxide are small at 430 K in the absence of methanol in the gas phase.

On ZrO_2/SiO_2, methoxide groups appear on both zirconia and silica when methanol adsorption occurs at 323 K. Methoxide on zirconia is formed by at least two routes. Gas-phase methanol can interact with hydroxyl groups on zirconia to form CH_3O–Zr and H_2O as evidenced by the spectra presented in Fig. 3. This route has been proposed previously by others (19, 21). Methanol can also dissociate at zirconia atoms to form CH_3O–Zr–H, as indicated by the Zr–H stretching mode observed at 1592 cm^{-1}. Another possible route to methoxide formation is the interaction of methanol with oxygen anions on zirconia to form methoxide on zirconia and hydroxyl groups on zirconia (19– 21). Methoxide formation by this route probably does not occur to a significant extent in the current study as hydroxyl groups are consumed and not generated during methanol adsorption (see Fig. 3).

As the temperature of methanol adsorption on ZrO_2/SiO_2 is increased to 523 K, no additional surface species are observed. A closely correlated reduction in methoxide concentration and recovery of hydroxyl groups is observed as the temperature is increased (see Fig. 4). The Zr–H stretching mode at 1592 cm^{-1} is also decreased in intensity with increasing temperature. This suggests that in the presence of methanol, the predominant processes occurring with increasing temperature are CH_3O–$Zr + H_2O \rightarrow CH_3OH + HO$–Zr and CH_3O–Zr–$H \rightarrow CH_3OH + Zr$. Upon prolonged purging in He at 523 K (125 h) the formation of b-HCOO–Zr is observed together with the depletion of CH_3O–Zr (see Figs. 5 and 6). These results indicate that the oxidation of CH_3O–Zr to b-HCOO–Zr at 523 K is an extremely slow process on ZrO_2/SiO_2. The appearance of m-CO_3–Zr together with the appearance of b-HCOO–Zr suggests that b-HCOO–Zr is further oxidized to m-CO_3–Zr during methanol decomposition on ZrO_2/SiO_2.

The carbon containing products observed during reaction of methanol with $Cu/ZrO_2/SiO_2$ are formaldehyde, which is observed to form at >325 K, CO_2 and CO, which form above 400 K, and methyl formate and dimethyl ether, observed to form above 460 K. The reaction by which formaldehyde is formed in the gas phase is proposed to be

$$CH_3OH + OH_{(a)} \rightarrow H_2CO + H_2O + 1/2H_2. \quad [10]$$

The TPD spectrum in Fig. 10 shows that H_2, H_2O, and CH_2O are simultaneously evolved, providing support for the above reaction. In reaction [10] water is formed by the interaction of methanol with OH groups on zirconia:

$$CH_3OH + OH_{(a)} \rightarrow CH_3O_{(a)} + H_2O. \quad [11]$$

This interaction is clearly evidenced in the spectra presented in Fig. 7, where at 323 K methanol exposure leads to features due to methoxide on zirconia and water adsorbed on silica, as well as negative peaks indicating the consumption of OH groups on zirconia. Hydrogen and formaldehyde are formed by the dehydrogenation of methoxide species on zirconia (reaction [3]), as suggested by the TPD of methanol, where considerably more formaldehyde is formed on $Cu/ZrO_2/SiO_2$ as compared to Cu/SiO_2 (see Table 1).

Carbon dioxide and CO formation observed above 400 K is attributed to the decomposition of formate species on Zr (19, 21):

$$HCOO_{(a)} \rightarrow CO_2 + 1/2H_2 \quad [12]$$

$$HCOO_{(a)} \rightarrow CO + OH_{(a)}. \quad [13]$$

The formate species on zirconia involved in reactions [12] and [13] are proposed to be derived by the interaction of adsorbed formaldehyde with OH groups on zirconia to form methylenebisoxy on zirconia with the liberation of atomic hydrogen. Methylenebisoxy is subsequently dehydrogenated to form formate species. Although methylenebisoxy species were not observed under the conditions of the present study, their formation has been observed during methanol synthesis from both CO_2 and CO on $Cu/ZrO_2/SiO_2$ (13, 14). Hence, the reactions by which CO_2 and CO are proposed to form from methanol are

$$CH_3OH + 2OH_{(a)} \rightarrow CO_2 + H_2O + 2H_2 \quad [14]$$

$$CH_3OH + OH_{(a)} \rightarrow CO + H_2O + 3/2H_2. \quad [15]$$

Formate species on zirconia are observed to form at 373 K (see Fig. 7), and CO_2 and H_2 are liberated in significant quantities above 400 K, giving maxima in the TPD spectra (see Fig. 10) at 495 K, at which temperature the decrease in the b-HCOO–Zr surface concentration with temperature is at a maximum (see Fig. 8). These results support the pathway indicated in reaction [12]. Evidence for b-HCOO–Zr decomposition to CO and OH groups can be derived from Fig. 12, where it is seen that significant quantities of CO are formed well below the temperature at which methyl formate formation, and hence possible decomposition, become appreciable. It is interesting to note that CO is not formed during the TPD of methanol on $Cu/ZrO_2/SiO_2$, although b-HCOO–Zr has been reported to decompose to both CO and CO_2 (21).

The origin of the methyl formate observed to form above 460 K is not determined. Although methyl formate on Cu is observed at 473 and 523 K (see Fig. 7), it is unclear whether this is due to the adsorption of gas-phase methyl formate on Cu, or due to methyl formate formation on Cu. It is clear that the gas-phase concentration of methyl formate observed during methanol TPR is much lower over $Cu/ZrO_2/SiO_2$ than over Cu/SiO_2, while the feature for adsorbed methyl formate on Cu is much stronger on $Cu/ZrO_2/SiO_2$ than on Cu/SiO_2, suggesting that zirconia stabilizes methyl formate on the Cu surface. Dimethyl ether formation observed above 460 K is again attributed to the dehydration of methanol and is more pronounced on the more acidic $Cu/ZrO_2/SiO_2$ than on Cu/SiO_2 (Figs. 11 and 12).

The formation of formate species on zirconia occurs already at 373 K on $Cu/ZrO_2/SiO_2$ (see Fig. 7), while only very slowly at 523 K on ZrO_2/SiO_2 (see Fig. 5). At 423 K and above, gas-phase CO_2 and CO–Cu are also observed in the infrared spectra presented in Fig. 7, which were not observed during methanol decomposition on ZrO_2/SiO_2 under the conditions studied. During the TPR of methanol on $Cu/ZrO_2/SiO_2$, gas-phase H_2, CO_2, and CO are also observed above 400 K (see Fig. 12), the formation of which is attributed to the decomposition of b-HCOO–Zr. This process has been observed to occur only above ~623 K on pure zirconia (21). The presence of Cu, therefore, enables the conversion of CH_3O–Zr to b-HCOO–Zr and the decomposition of b-HCOO–Zr to CO_2, CO, and H_2 to occur at lower temperatures than in the absence of Cu.

Our investigations of methanol synthesis from CO_2/H_2 on the same catalysts as used in this study have shown that b-HCOO–Zr and CH_3O–Zr are formed at lower temperatures and at higher rates on $Cu/ZrO_2/SiO_2$ than on ZrO_2/SiO_2 (13). In that case it was suggested that the hydrogen required for these hydrogenation reactions to take place is supplied by spillover from Cu to the intermediates located on zirconia. In the present case, the conversion of CH_3O–Zr to b-HCOO–Zr requires a source of oxygen and a sink for hydrogen to proceed. The source of oxygen is proposed to be hydroxyl groups on zirconia. The sink for hydrogen is proposed to be Cu, where it is assumed that hydrogen is transferred from zirconia to Cu by reverse spillover. In the absence of Cu, this sink for hydrogen is unavailable, and hence methoxide conversion is not observed to be facile under the conditions of this study. In the presence of Cu, hydrogen transfer from zirconia to Cu is available allowing for the conversion of methoxide to formate and subsequent formate decomposition to CO, CO_2, and H_2 to occur more readily.

A proposed mechanism for methanol decomposition on the zirconia component of $Cu/ZrO_2/SiO_2$ is shown in Fig. 15. Methanol interacts with OH groups on zirconia to form

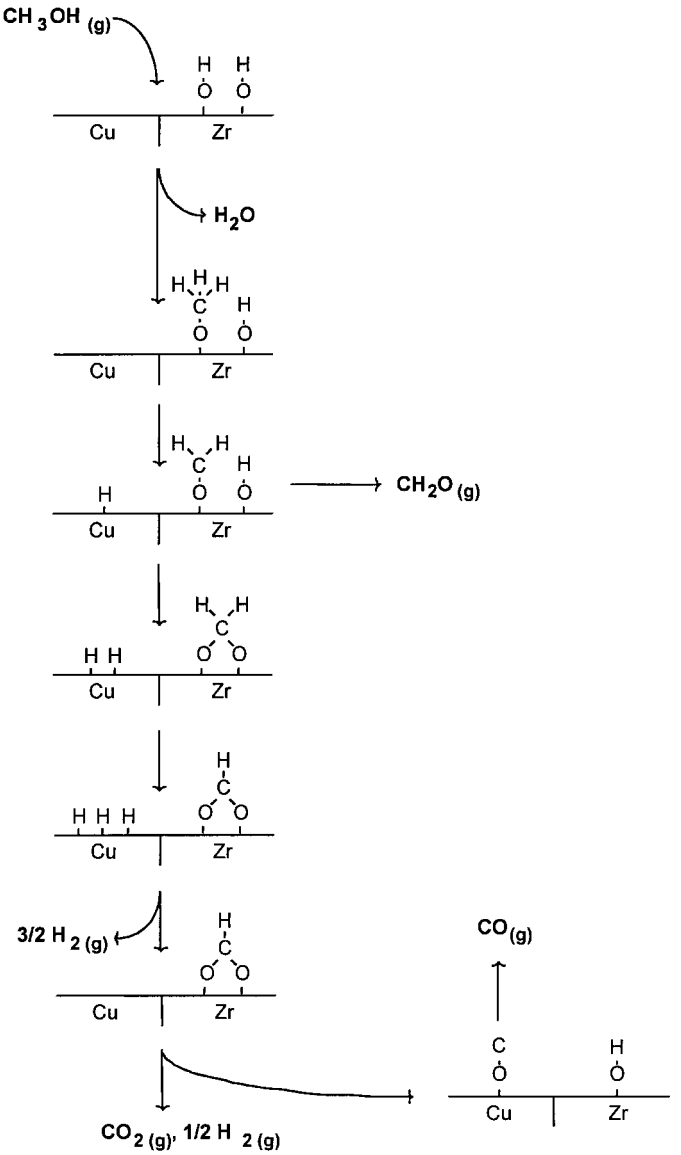

FIG. 15. Proposed mechanism for the decomposition of methanol on $Cu/ZrO_2/SiO_2$.

methoxide and water. The dehydrogenation of methoxide is proposed to lead to adsorbed formaldehyde on zirconia, which reacts with OH groups on zirconia to form methylenebisoxy on zirconia, with the liberated atomic hydrogen being transferred to the Cu surface. Dehydrogenation of methylenebisoxy results in the formation of bidentate formate on zirconia at 373 K with the further liberation of atomic hydrogen. Formate species on zirconia are decomposed above 400 K, resulting in either gas-phase CO_2 and hydrogen generation or CO and zirconia hydroxyl group formation. The primary role of copper is the acceptance of hydrogen released from surface species located on zirconia and the subsequent desorption of molecular hydrogen.

The relative effectiveness of Cu/SiO_2 as compared to $Cu/ZrO_2/SiO_2$ for methanol decomposition can be surmised from the data presented in Table 1. During the TPD of methanol approximately twice as much CO_2 and six times as much CH_2O are formed on $Cu/ZrO_2/SiO_2$ as compared to Cu/SiO_2, indicating that more preadsorbed methanol decomposes on $Cu/ZrO_2/SiO_2$ than on Cu/SiO_2.

CONCLUSIONS

The decomposition of methanol on Cu/SiO_2 leads to predominantly CO, CO_2, H_2, and methyl formate formation in the presence of gas-phase methanol. CO_2 and H_2 are liberated as formate species on Cu are decomposed, while CO and H_2 are formed from the decomposition of methyl formate. In the absence of gas-phase methanol, adsorbed methanol is primarily decomposed to CO_2 and H_2 as formate species are decomposed. During the decomposition of methanol on $Cu/ZrO_2/SiO_2$, CO, CO_2, and H_2 the principal products resulting from the decomposition of formate species on zirconia above ~400 K are formed. More preadsorbed methanol is decomposed on $Cu/ZrO_2/SiO_2$ than on Cu/SiO_2.

On both catalysts, methoxide species are formed near ambient temperature, formate species are observed at 373 K, and gas-phase decomposition products are observed near 400 K. In the presence of zirconia, methoxide and formate intermediates are located on zirconia, while on Cu/SiO_2 these intermediates are coordinated to Cu. The decomposition of methanol on ZrO_2/SiO_2 proceeds only very slowly at 523 K. The addition of Cu to ZrO_2/SiO_2 produces a catalyst which efficiently decomposes methanol above 400 K. It is proposed that Cu provides a route for the removal of hydrogen produced during methanol decomposition, by reverse spillover of atomic hydrogen from zirconia to Cu, and the subsequent desorption of molecular hydrogen from Cu. Thus the presence of Cu plays a similar role during methanol decomposition as for methanol synthesis on $Cu/ZrO_2/SiO_2$. In the case of methanol synthesis, the role of Cu is to dissociate and provide atomic hydrogen to zirconia by spillover, while during methanol decomposition, Cu serves as a sink for atomic hydrogen and to liberate molecular hydrogen by recombinative desorption.

ACKNOWLEDGMENT

The authors acknowledge Hee-Chul Woo and Johan Agrell for their assistance with these studies. This work was supported by the Director, Office of Basic Energy Sciences, Chemical Sciences Division, of the U.S. Department of Energy under Contract DE-AC03-76SF00098.

REFERENCES

1. Bartley, G. J. J., and Burch, R., *Appl. Catal.* **43**, 141 (1988).
2. Denise, B., and Sneeden, R. P. A., *Appl. Catal.* **28**, 235 (1986).
3. Chen, H. W., White, J. M., and Ekerdt, J. G., *J. Catal.* **99**, 293 (1986).
4. Amenomiya, Y., *Appl. Catal.* **30**, 57 (1987).
5. Denise, B., Sneeden, R. P. A., Beguin, B., and Cherifi, O., *Appl. Catal.* **30**, 353 (1987).
6. Koeppel, R. A., Baiker, A., Schild, C., and Wokaun, A., *Stud. Surf. Sci. Catal.* **63**, 59 (1991).
7. Kanoun, N., Astier, M. P., and Pajonk, G. M., *Catal. Lett.* **15**, 231 (1992).
8. Koeppel, R. A., Baiker, A., and Wokaun, A., *Appl. Catal. A* **84**, 77 (1992).
9. Sun, Y., and Sermon, P. A., *J. Chem. Soc., Chem. Commun.* 1242 (1993).
10. Nitta, Y., Suwata, O., Ikeda, Y., Okamoto, Y., and Imanaka, T., *Catal. Lett.* **26**, 345 (1994).
11. Sun, Y., and Sermon, P. A., *Catal. Lett.* **29**, 361 (1994).
12. Fisher, I. A., Woo, H. C., and Bell, A. T., *Catal. Lett.* **44**, 11 (1997).
13. Fisher, I. A., and Bell, A. T., *J. Catal.* **172**, 222 (1997).
14. Fisher, I. A., and Bell, A. T., *J. Catal.* **178**, 153 (1998).
15. Millar, G. J., Rochester, C. H., and Waugh, K. C., *J. Chem. Soc. Faraday Trans.* **87**, 2795 (1991).
16. Clarke, D. B., Lee, D. K., Sandoval, M. J., and Bell, A. T., *J. Catal.* **150**, 81 (1994).
17. He, M. Y., and Ekerdt, J. G., *J. Catal.* **87**, 238 (1984).
18. He, M. Y., and Ekerdt, J. G., *J. Catal.* **87**, 381 (1984).
19. Hussein, A. M., Sheppard, N., Zaki, M. I., and Fahim, R. B., *J. Chem. Soc. Faraday Trans.* **87**, 2655 (1991).
20. Dilara, P. A., and Vohs, J. M., *Surf. Sci.* **321**, 8 (1994).
21. Bianchi, D., Chafik, T., Khalfallah, M., and Teichner, S. J., *Appl. Catal. A* **123**, 89 (1995).
22. Hicks, R. F., Kellner, C. S., Savatsky, B. J., Hecker, W. C., and Bell, A. T., *J. Catal.* **71**, 216 (1981).
23. Monti, D. M., Cant, N. W., Trimm, D. L., and Wainwright, M. S., *J. Catal.* **100**, 17 (1986).
24. Wovchko, E. A., Camp, J. C., Glass, J. A., and Yates, J. T., *Langmuir* **11**, 2592 (1995).
25. Pritchard, J., Catterick, T., and Gupta, R. K., *Surf. Sci.* **53**, 1 (1975).
26. Millar, G. J., Rochester, C. H., and Waugh, K. C., *J. Chem. Soc. Faraday Trans.* **87**, 1491 (1991).
27. Weigel, J., Koeppel, R. A., Baiker, A., and Wokaun, A., *Langmuir* **12**, 5319 (1996).
28. Kondo, J., Abe, H., Sakata, Y., Maruya, K., Domen, K., and Onishi, T., *J. Chem. Soc. Faraday Trans. 1* **84**, 511 (1988).
29. Guglielminotti, E., *Langmuir* **6**, 1455 (1990).
30. Chafik, T., Bianchi, D., and Teichner, S. J., *Top. Catal.* **2**, 103 (1995).
31. He, M. Y., and Ekerdt, J. G., *J. Catal.* **90**, 17 (1984).
32. Millar, G. J., Rochester, C. H., Howe, C., and Waugh, K. C., *Mol. Phys.* **76**, 833 (1991).
33. Manriquez, J. M., McAlister, D. R., Sanner, R. D., and Bercaw, J. E., *J. Am. Chem. Soc.* **98**, 6733 (1976).
34. Hertl, W., *Langmuir* **5**, 96 (1989).

35. Argon, P. A., Fuller, E. L., and Holmes, H. F., *J. Colloid Interface Sci.* **52**, 553 (1975).
36. Bianchi, D., Chafik, T., Khalfallah, M., and Teichner, S. J., *Appl. Catal. A* **105**, 223 (1993).
37. Bianchi, D., Chafik, T., Khalfallah, M., and Teichner, S. J., *Appl. Catal. A* **101**, 297 (1993).
38. Bianchi, D., Chafik, T., Khalfallah, M., and Teichner, S. J., *Appl. Catal. A* **112**, 57 (1994).
39. Bianchi, D., Chafik, T., Khalfallah, M., and Teichner, S. J., *Appl. Catal. A* **112**, 219 (1994).
40. Morterra, C., and Orio, L., *Mat. Chem. and Phys.* **24**, 247 (1990).
41. Sexton, B., *Surf. Sci.* **88**, 299 (1979).
42. Wachs, I. E., and Madix, R. J., *J. Catal.* **53**, 208 (1978).
43. Sexton, B., Hughes, A. E., and Avery, N. R., *Surf. Sci.* **155**, 366 (1985).
44. Russell, J. N., Gates, S. M., and Yates, J. T., *Surf. Sci.* **163**, 516 (1985).
45. Chauvin, C., Saussey, J., Lavalley, J. C., Idriss, H., Hindermann, J. P., Kiennemann, A., Chaumette, P., and Courty, P., *J. Catal.* **121**, 56 (1990).
46. Bowker, M., Hadden, R. A., Houghton, H., Hyland, J. N. K., and Waugh, K. C., *J. Catal.* **109**, 263 (1988).
47. Evans, J. W., Wainright, M. S., Bridgewater, A. J., and Young, D. J., *Appl. Catal.* **7**, 75 (1983).
48. Van der Grift, C. J. G., Mulder, A., and Geus, J. W., *Appl. Catal.* **60**, 181 (1990).
49. Chinchen, G. C., Spencer, M. S., Waugh, K. C., and Whan, D. A., *J. Chem. Soc. Faraday Trans. 1* **83**, 2193 (1987).
50. Chinchen, G. C., and Spencer, M. S., *J. Catal.* **112**, 325 (1988).
51. Au, C. T., Breza, J., and Roberts, M. W., *Chem. Phys. Lett.* **66**, 340 (1979).
52. Barnes, C., Pudney, P., Guo, Q., and Bowker, M., *J. Chem. Soc. Faraday Trans.* **87**, 1491 (1991).
53. Chen, A. K., and Masel, R., *Surf. Sci.* **343**, 17 (1995).
54. Sexton, B., *Surf. Sci.* **88**, 319 (1979).
55. Ying, D. H. S., and Madix, R. J., *J. Catal.* **61**, 48 (1980).
56. Iglesia, E., and Boudart, M., *J. Catal.* **81**, 214 (1983).
57. Clarke, D. B., Suzuki, I., and Bell, A. T., *J. Catal.* **142**, 27 (1993).
58. Monti, D. M., Cant, N. W., Trimm, D. L., and Wainwright, M. S., *J. Catal.* **100**, 28 (1986).
59. Minachev, K. M., Kotyaev, K. P., Lin, G. I., Rozovskii, A. Y., *Catal. Lett.* **3**, 299 (1989).